═══════ *Optoelectronics and optoelectronic devices* ═══════

Key parameters of textured silicon solar cells of 26.6% photoconversion efficiency

A.V. Sachenko[1], V.P. Kostylyov[1], R.M. Korkishko[1], V.M. Vlasyuk[1], I.O. Sokolovskyi[1], B.F. Dvernikov[1], V.V. Chernenko[1], and M. Evstigneev[2]

[1]*V. Lashkaryov Institute of Semiconductor Physics, NAS of Ukraine*
45, prospect Nauky, 03680 Kyiv, Ukraine
[2]*Memorial University of Newfoundland, St. John's, NL, A1B 3X7, Canada*
E-mail: sach@isp.kiev.ua; viktorvlasiuk@gmail.com

Abstract. A new approach to modeling the parameters of high efficiency textured silicon solar cells (SCs) has been presented. Unlike conventional optimization formalisms, our approach additionally includes such important factors as the non-radiative Auger recombination of excitons *via* deep impurity levels as well as electron-hole pairs recombination in the space charge region. A simple phenomenological expression offered by us earlier for the external quantum efficiency of the textured silicon solar cells with account of the photocurrent in the long-wave part of the absorption spectrum has been also used. Applying this approach, the key parameters of textured silicon SCs, namely: short-circuit current, open-circuit voltage and photoconversion efficiency, have been theoretically determined. The proposed formalism allows calculating the thickness dependence of photoconversion efficiency, which is in good agreement with the experimental results obtained for the heterojunction SCs with the record photoconversion efficiency of 26.6%. The offered approach and the results of applying this phenomenological expression for the external quantum efficiency of the photocurrent in the long-wave part of the absorption spectrum can be used to optimize the characteristics of high efficiency textured SCs based on monocrystalline silicon.

Keywords: silicon solar cell, texture, open circuit voltage, short circuit current density, photoconversion efficiency, fill factor.

1. Introduction

Improving the photoconversion efficiency is a key scientific and practical task in researching the solar cells (SCs). It is achieved by reducing the bulk and surface recombination rates and optical losses due to light reflection from the front surface. The bulk recombination rate is decreased by lowering the SC base thickness and by using high-purity silicon with low concentrations of deep impurities responsible for Shockley–Reed–Hall recombination. The surface recombination velocity is lowered by using an isotype transition or a heterojunction at the rear SC surface, as well as by surface passivation with thermal silicon oxide or embedding hydrogen into the semiconductor. Finally, a radical method of decreasing the light reflection coefficient is by texturing the front surface of the silicon wafer.

The purpose of this work is to refine the existing models of silicon SCs by accounting for two effects that are usually neglected. The first one is the nonradiative exciton Auger recombination assisted by deep impurities. Its existence has been unequivocally demonstrated by Hangleiter [1, 2], and its contribution to the net recombination rate is comparable to other recombination channels. In the monograph [3], a detailed analysis of the works [1, 2] was performed from the standpoint of manifestation of this recombination mechanism. The second effect is recombination in the space-charge region (SCR), which likewise significantly affects the characteristics of highly efficient silicon SCs.

In the literature, when considering recombination in SCR, the dependences of generation-recombination current on the applied voltage are usually analyzed. In SCs, it is necessary to compare the contributions of different recombination components of the flowing current depending on the excess concentration of electron-hole pairs. In this work such analysis is carried out. In this case, certain complications arise when the excess concentration of electron-hole pairs exceeds the equilibrium concentration of the majority charge carriers

in the base. As shown in this paper, these complications can be overcome, when the distribution of the inverse lifetime of non-equilibrium carriers in SCR is described by Gaussian.

The theory described below is a one-dimensional approximation, which allows obtaining the values of the photoconversion efficiency and other SC parameters, namely: the short-circuit current, open-circuit voltage, and fill factor of the I–V curve. It is valid, if two criteria are fulfilled: (i) the diffusion length must be much greater than the base thickness, $L_d >> d$; (ii) the net (front plus rear) surface recombination velocity must be much smaller than the ratio of the ambipolar diffusion coefficient to the base thickness, $S_s << D_A/d$. Then, the spatial dependence of the excess concentration of carriers can be neglected. Silicon SCs with the photoconversion efficiency above 20% have a lifetime of more than 1 ms and surface recombination velocity in the cm/s range. Therefore, they meet both criteria very well.

The results of this theoretical modeling are compared with the experimental results obtained in the work [4, 5] that reports the highest photoconversion efficiency for silicon SCs obtained up to date, which at the time of publication was 26.6%, and recently increased to 26.7% [6]. A good agreement with the experimental results is obtained. It is suggested that efficiency decrease with lowering the excess concentration, Δn, at its low values may have to do with recombination in the space charge region.

2. External quantum efficiency and the light-generated current

The external quantum efficiency $EQE(\lambda)$ allows one to determine the current density generated by the incident radiation with the spectral photon flux $I(\lambda)$ as

$$J_L = q \int EQE(\lambda)\, I(\lambda) d\lambda , \qquad (1)$$

where q is the elementary charge. The value of $EQE(\lambda)$ is determined by such factors as the chemical composition and morphology of the semiconductor surface coated with transparent conductive or translucent layers or a grid for current collection, the light absorption coefficient in the semiconductor, *etc.*

The external quantum efficiency is given by the product of absorbance, $A(\lambda)$, and the probability for a photon to enter the SC, which is unity minus the reflection coefficient, $EQE = A\,(1 - R)$. In [7, 8], a theoretical approach is introduced, which allows obtaining J_{SC} from the experimental $R(\lambda)$ curve and a fitting expression for $A(\lambda)$ that involves three parameters. We used a simplified approach [9, 10], in which the short-circuit current is represented by a sum of two contributions:

$$J_L(d,b) = q\left[\int_{\lambda_0}^{800} I(\lambda) EQE_s(\lambda) d\lambda + \int_{800}^{1200} I(\lambda) EQE_l(\lambda,b) d\lambda \right] \quad (2)$$

The $EQE(\lambda)$ curve in the long-wave (subscript *l*) part of the spectrum, $\lambda > 800$ nm, is fitted with a

phenomenological formula that involves two fit parameters, *f* and *g*:

$$EQE_l(\lambda,d) = \frac{f}{1 + \left(g\alpha(\lambda)d\right)^{-1}} , \qquad (3)$$

where d is the base thickness and $\alpha(\lambda)$ is the absorption coefficient. In [9, 10], the fit parameter g was expressed in terms of another fit parameter, b, as $g = 4n_r^2/b$. Given that the refractive index, $n_r(\lambda)$, depends only weakly on the wavelength in this part of the spectrum, the two fitting expressions are practically the same.

In the short-wave part of the spectrum, $\lambda < 800$ nm (subscript *s*), the $EQE(\lambda)$ curve does not depend on the thickness. Rather, it is determined by the reflection losses, shading and light absorption outside the base region. Hence, $EQE_s(\lambda)$ at any base thickness is determined from the experimental plot measured for one base thickness value. The values of $EQE_l(800$ nm) and $EQE_s(800$ nm) must be the same, which allows to determine the parameter *f*.

Fig. 1 shows the experimental $EQE(\lambda)$ curve from [4] and fit $EQE_l(\lambda)$ counterpart. The agreement between the experiment and the theory is achieved for $g = 27.9$ and $f = 0.99$.

3. Recombination mechanisms

The total lifetime in SC τ_{eff} is formed by the intrinsic – radiative and Auger – and extrinsic recombination mechanisms τ_{extr}. The latter includes the Shockley–Reed–Hall recombination with the lifetime τ_{SRH}, the non-radiative exciton Auger recombination *via* a deep recombination level [11] with the lifetime τ_{exc}^n, surface recombination and recombination in the space charge region with the combined lifetime τ_{eff}^s:

$$\tau_{eff}^{-1} = \tau_{rad}^{-1} + \tau_{Auger}^{-1} + \tau_{SRH}^{-1} + \left(\tau_{exc}^n\right)^{-1} + \left(\tau_s\right)^{-1} + \left(\tau_{SCR}\right)^{-1} \quad (4)$$

$$\tau_{extr}^{-1} = \tau_{SRH}^{-1} + \left(\tau_{exc}^n\right)^{-1} + \left(\tau_s\right)^{-1} + \left(\tau_{SCR}\right)^{-1} . \qquad (4a)$$

The radiative recombination lifetime is given by [12]

$$\tau_{rad}^{-1} = B\,(1 - P_{PR})\,(n_0 + \Delta n) , \qquad (5)$$

where B is the radiative recombination coefficient, P_{PR} – re-absorption probability, n_0 – equilibrium electron concentration, and Δn – excess electron-hole pair concentration. Radiative recombination coefficient B is expressed by the formula [12]

$$B = \int_0^\infty B(E)dE , \quad B(E) = \left(\frac{n_r(E)\,\alpha(E)\,E}{\pi\,c\,\hbar^{3/2}\,n_i}\right)^2 e^{-E/k_B T} , \quad (6)$$

in which $n_r(E)$ and $\alpha(E)$ are the refractive index and absorption coefficient as functions of photon energy $E = hc/\lambda$. The photon re-absorption probability is given by

$$P_{PR} = B^{-1} \int_0^\infty A(E)\,B(E)dE . \qquad (7)$$

Sachenko A.V., Kostylyov V.P., Korkishko R.M. et al. Key parameters of textured silicon solar cells of 26.6% …

176

The absorbance is given by the same expression as (3), except for the factor f in the numerator is replaced with unity [10]:

$$A = \frac{1}{1 + \left(g\alpha(\lambda)d\right)^{-1}} . \tag{8}$$

For the band-to-band Auger recombination lifetime, we used the empirical expression from [12, 13].

The Shockley–Reed–Hall lifetime as a function of the doping and excitation levels is given by the standard formula

$$\tau_{\text{SRH}} \cong \frac{\tau_{p0}\left(n_0 + n_1 + \Delta n\right) + \tau_{n0}\left(p_1 + \Delta n\right)}{\left(n_0 + \Delta n\right)} . \tag{9}$$

Here, the characteristic times $\tau_{p0} = \left(V_p \sigma_p N_t\right)^{-1}$ and $\tau_{n0} = \left(V_n \sigma_n N_t\right)^{-1}$ are expressed in terms of the hole and electron thermal velocities V_p and V_n, their capture cross-sections σ_p and σ_n by the deep traps of concentration N_t. Finally, n_1 and p_1 are the electron and hole equilibrium concentrations in the case when the Fermi energy coincides with the energy level of the trap. Depending on the excess concentration Δn of the electron-hole pairs, the τ_{SRH}-value varies between the low-injection and the high-injection limits. In particular, for SCs with the n-type base, the value of τ_{SRH} increases with Δn for $\sigma_p > \sigma_n$ and is practically constant for $\sigma_p < \sigma_n$.

The non-radiative exciton Auger recombination time, according to [11], is equal to

$$\tau_{exc}^n = \tau_{\text{SRH}} \frac{n_x}{n_0 + \Delta n} \tag{10}$$

with $n_x = 8.2 \cdot 10^{15}$ cm^{-3}.

The surface and SCR recombination time is defined as

$$\tau_s = d/S_s , \quad \tau_{SCR} = d/S_{SCR} , \tag{11}$$

where S_s is the net recombination velocity on the front and the rear surfaces, and S_{SCR} is the SCR recombination velocity. For the former, we use the fitting expression [10]

$$S_s = S_{0s} \left(\frac{n_0}{n_p}\right)^m \left(1 + \frac{\Delta n}{n_0}\right)^r , \tag{12}$$

where S_{0s} is the net recombination velocity at $\Delta n = 0$, n_p – fit parameter to ensure dimensional consistency, the exponents m and r are both close to unity; however, in some cases the parameter r may be bigger or lower than unity.

The SCR recombination velocity is given by

Fig. 1. Experimental external quantum efficiency from [4] (symbols) and theoretical fit (line).

Here, $b_r = V_p \sigma_p^* / V_n \sigma_n^*$, the asterisk refers to the SCR parameters, $\tau_{SCR}(x) = \left(V_p \sigma_p^* N_t^*(x)\right)^{-1}$, N_t^* is the concentration of traps in SCR, $y(x)$ – electric potential normalized to the thermal voltage, and E_t^* – trap energy measured from the middle of the bandgap.

A good agreement between the experiment and the theory can be obtained by assuming a Gaussian dependence of the inverse lifetime,

$$\tau_{SCR}^{-1}(x) = \tau_m^{-1} \exp\left(\frac{-\left(x - x_m\right)^2}{2\sigma^2}\right) , \tag{14}$$

with fit parameters x_m, σ and τ_m. The upper integration limit w in (13) must be of the order of $x_m + 5\sigma$ to make sure that the Gaussian (14) at $x = w$ is practically zero.

To find the dependence of the non-dimensional potential on the coordinate, it is necessary to use the solution of the Poisson equation

$$x = \sqrt{\frac{\varepsilon_0 \varepsilon_{\text{Si}} kT}{2q^2 n_0}} \int_{y_0}^{y} \frac{dy_1}{\sqrt{\left(1 + \frac{\Delta n}{n_0}\right)\left(e^{y_1} - 1\right) - y_1 + \frac{\Delta n}{n_0}\left(e^{-y_1} - 1\right)}} . \tag{15}$$

where q is the elementary charge, ε_0 – vacuum permittivity, and ε_{Si} – dielectric constant of Si. The initial value of the potential, $y_0 = y(x = 0)$, is found by modeling the n-p^+ junction on the p^+-side as a thin negatively charged slab with the surface charge density $-qN$, N being the surface concentration of acceptor ions in that slab. Then, from the Poisson equation, we find

$$N = \frac{1}{q} \sqrt{2kT\varepsilon_0 \varepsilon_{\text{Si}} \left[\left(n_0 + \Delta n\right)\left(e^{y_0} - 1\right) - n_0 y_0 + \Delta n\left(e^{-y_0} - 1\right)\right]} . \tag{16}$$

$$S_{SCR}(\Delta n) = \int_0^w \frac{\left(n_0 + \Delta n\right)dx}{\left[\left(n_0 + \Delta n\right)e^{y(x)} + n_i(T)e^{E_t^*/kT} + b_r\left(\left(p_0 + \Delta n\right)e^{-y(x)} + n_i(T)e^{-E_t^*/kT}\right)\right]\tau_{SCR}(x)} . \tag{13}$$

Sachenko A.V., Kostylyov V.P., Korkishko R.M. et al. Key parameters of textured silicon solar cells of 26.6% ...

In most materials used to manufacture textured silicon SCs, the curves of $\tau_{SRH}(\Delta n)$ and $\tau_{eff}(\Delta n)$ typically saturate in the region of $\Delta n < 10^{15}$ cm^{-3} (see, *e.g.* [10, 12]). In contrast, in the finished silicon SCs $\tau_{eff}(\Delta n)$ decreases in this range with decreasing Δn [4, 14]. How can one understand this difference? In the crystalline Si samples used for measurements, there is no *p-n* junction. On both surfaces of the sample, the band bending is symmetric and, as a rule, slightly exhausting due to the passivation treatment to which the wafers were subjected before measuring the bulk lifetime. On the other hand, SCs have a *p-n* junction close to one of the surfaces. In this case, the recombination in the near-surface SCR is significant. In the studies [15, 16] it was shown that the region on the dark recombination current *vs* the applied voltage curve in silicon SCs is determined by the SCR recombination, when the non-ideality factor is close to 2. This is so not only at small applied voltages, but up to the voltage at the maximal power $V_m = 0.55 - 0.65$ V [16]. This can be explained by the fact that the value of Shockley–Reed–Hall lifetime in SCR is always significantly less than in the quasi-neutral bulk region. This, in turn, is due to the fact that the concentration of deep traps is much higher in SCR than in the bulk.

It should be noted that the decrease of $\tau_{eff}(\Delta n)$ with decreasing Δn can also be observed in the absence of recombination in SCR, provided that τ_{SRH} increases with increasing Δn, which is possible if $\sigma_p \geq \sigma_n$. At the end of the work, this case will be analyzed.

4. Photoconversion efficiency modeling for AM1.5 irradiation

We consider SC based on a p^+-n-n^+ structure. If the minority carriers' diffusion length $L_d = \sqrt{D_p \tau_{eff}}$ is much larger than one-quarter of the base thickness $d/4$, and if the combined surface and SCR recombination velocity $S_{SCR} + S_S << 2D_p/d$, then the excess concentration profile is practically uniform in the base region. In that case, one can employ the narrow-base approximation and express the illuminated *I–V* relation as [14]

$$I(V) = I_L - \frac{qA_{SC}d\,\Delta n}{\tau_{eff}(\Delta n)} - \frac{V + IR_s}{R_{sh}}, \qquad (17)$$

where the first term is the light-generated current, the second term – recombination current, A_{SC} – SC area, and R_s and R_{sh} are the series and shunt resistances, respectively.

The expression for dark current according to (17) has the form

$$I_D(V) = \frac{qA_{SC}d\,\Delta n}{\tau_{eff}(\Delta n)} + \frac{V - I_D R_s}{R_{sh}}. \qquad (18)$$

The excess carrier concentration is related to the applied voltage by a modified acting mass law,

$$(n_0 + \Delta n)(p_0 + \Delta n) = n_{i0}^2 \exp\left(\frac{\Delta E_g + q(V - IR_s)}{kT}\right), \qquad (19)$$

where n_{i0} is the intrinsic concentration at low injection [17], and $\Delta E_g(n_0, \Delta n)$ – magnitude of bandgap narrowing in Si [18]. Eq. (19) can be solved for the excess concentration

$$\Delta n = -\frac{n_0}{2} + \sqrt{\frac{n_0^2}{4} + n_{i0}^2 e^{\Delta E_g / kT}\left(e^{q(V - IR_s)/kT} - 1\right)}. \qquad (20)$$

Equations (17), (20) need to be solved numerically.

The relationship between the excess concentration Δn_{OC} in the open-circuit mode and the open-circuit voltage V_{OC} is obtained from the equation (20), if we put in it $\Delta n = \Delta n_{OC}$, $V = V_{OC}$ and $I = 0$, then:

$$\Delta n_{OC} = -\frac{n_0}{2} + \sqrt{\frac{n_0^2}{4} + n_{i0}^2 e^{\Delta E_g / kT}\left(e^{qV_{OC}/kT} - 1\right)}, \qquad (21)$$

The second relationship between them can be obtained from (17), if we put in it $I = 0$:

$$I_L = \frac{A_{SC}\,qd}{\tau_{eff}(\Delta n_{OC})}\Delta n_{OC} + \frac{V_{OC}}{R_{sh}}. \qquad (22)$$

Here, $\tau_{eff}(\Delta n_{OC})$ is found using (4).

The photoconversion efficiency η, as well as the voltage V_m, current I_m, and output power P_m in the maximum-power operation regime are found by setting the derivative of $P = IV$ to be zero with respect to voltage.

If we compare the expressions for Δn and Δn_{OC}, as well as the expressions for dark current (18) and photogeneration current (22), we can see that they coincide when we replace V by V_{OC}, I_D by I_L, and put R_s in (20) equal to zero. This means that solutions $I_D(V, R_{sh}, R_s)$ and $I_L(V_{OC}, R_{sh})$ are identical if $R_s = 0$.

5. Comparison of theoretical modeling with experimental results

Next, we present the results of theoretical modeling of the characteristics of textured SCs based on monocrystalline silicon described in [4]. The studied SCs had the structure a-Si:H-Si, and the current-collecting contacts in them were produced on the rear side. The key experimental curves presented in the work [4] were the external quantum efficiency *vs* the wavelength $EQE(\lambda)$, the effective lifetime on the excess concentration of electron-hole pairs $\tau_{eff}(\Delta n)$, the *I–V* curves for the case of illumination, and the curves of the open-circuit voltage as dependent on the incident intensity with the AM1.5 spectrum. According to the results presented earlier, the $EQE(\lambda)$ curves obtained in this work by using the empirical formula (4) were used to calculate the photogenerated current density J_L. For theoretical modeling of the experimental curves, it was necessary to determine a number of unknown parameters, which are not given in [4]. These are the Shockley–Reed–Hall lifetime, surface recombination rate, Gaussian parameters that define the lifetime in SCR, the ratio of the capture cross-sections for holes and electrons, the shunt resistance and the series resistance.

Sachenko A.V., Kostylyov V.P., Korkishko R.M. et al. Key parameters of textured silicon solar cells of 26.6% ...

178

To determine the effective lifetime *vs* the excitation level, Yoshikawa *et al.* [4] measured the open-circuit voltage and the short-circuit current for different illumination intensities. When analyzing their experimental data, they did not take into account the bandgap narrowing effect. As a result, the excess concentration in Yoshikawa *et al.* [4] paper, Δn_Y, turned out to be slightly underestimated at $\Delta n > 10^{15}$ cm^{-3}. To relate the excess concentration Δn_Y from Yoshikawa's paper [4] and to more accurate estimate the Δn value, we note that the former is given by the following expression (cf. Eq. (1) in [5]):

$$\Delta n_Y = -\frac{n_0}{2} + \sqrt{\frac{n_0^2}{4} + n_{i0}^2 \left(e^{qV_{OC}/kT} - 1\right)} . \quad (23)$$

The bandgap narrowing $\Delta E_g(\Delta n)$ increases with Δn, but in the relevant parameter range ($\Delta n < 2 \cdot 10^{16}$ cm^{-3}) it does not exceed 0.004 eV ~ 0.15kT. This allows one to linearize the difference between the expressions (21) and (23) with respect to a small parameter $\Delta E_g/kT$ to obtain a simple expression to improve the accuracy of Yoshikawa's *et al.* estimate for Δn:
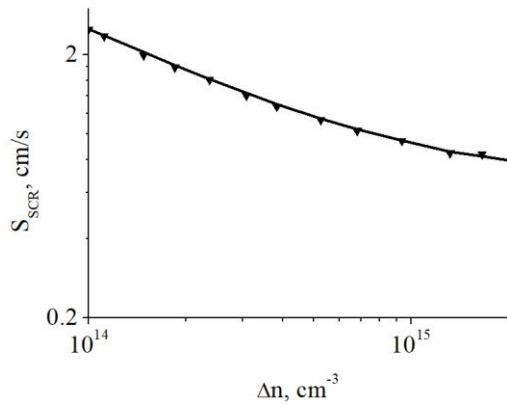
Fig. 2. Experimental (symbols) and calculated (line) SCR recombination velocity *vs* excitation level.
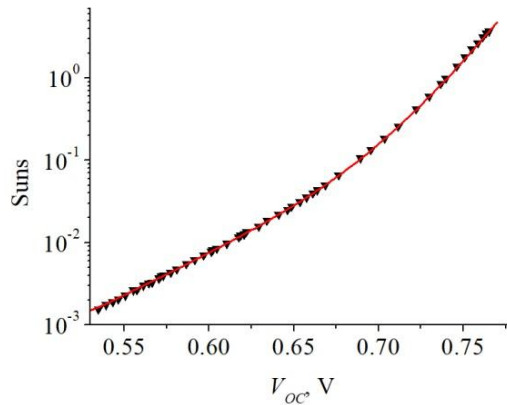
Fig. 3. Illumination *vs* open-circuit voltage. Symbols: experiment [4], solid line: theoretical fitting.

$$\Delta n_{OC} - \Delta n_Y =$$
$$= \frac{\Delta E_g(\Delta n_{OC})}{kT} \frac{\Delta n_Y(N_d + \Delta n_Y) - n_{i0}^2}{\sqrt{N_d^2 + 4\left(\Delta n_Y(N_d + \Delta n_Y) - n_{i0}^2\right)}} = \quad (24)$$
$$= \frac{\Delta E_g(\Delta n_Y)}{kT} \frac{\Delta n_Y(N_d + \Delta n_Y)}{\sqrt{N_d^2 + 4\Delta n_Y(N_d + \Delta n_Y)}} .$$

In the latter equality, we neglected the intrinsic concentration squared and replaced Δn_{OC} with Δn_Y in the argument of ΔE_g, keeping in mind that the difference between the two estimates for Δn should be quite small.

From the experimental effective lifetime as a function of Δn (see Fig. 4a in [4]), one can determine the "experimental" recombination velocity in SCR, $S_{SCR}^{exp}(\Delta n)$. For this, one needs the parameters τ_{SRH}, S_{0s}, and r, which can be determined from a comparison between the theoretical and experimental I–V and $\tau_{eff}(\Delta n)$ curves from [4]. Then, one can use the following expression:

$$S_{SCR}^{exp}(\Delta n) = \left[\left(\tau_{eff}^{exp}\right)^{-1} - \left(\tau_{SRH}^{-1} + \tau_{exc}^{n}{}^{-1} + \tau_s^{-1} + \tau_{rad}^{-1} + \tau_{Auger}^{-1}\right)\right]d. \quad (25)$$

Upon substitution of the obtained $\tau_{eff}(\Delta n)$ value into (23), we obtain the SCR recombination velocity as a function of the excitation level, see Fig. 2 (symbols). The corresponding curve calculated using (11)–(14) is shown in Fig. 2 as a solid line. The fitting parameters are summarized in Table. The agreement between the experimental and the fitted curves within the range 10^{14} cm^{-3} < Δn < 10^{16} cm^{-3} is obvious. In their turn, the parameters of Gaussian (14) were found by fitting the $\tau_{eff}(\Delta n)$ curve in the Δn-region to the left of the maximum.
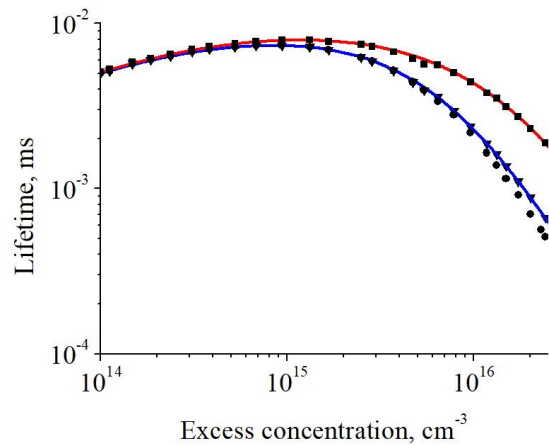
Fig. 4. The effective lifetime as extracted from the experimental data [4] (circles), the corrected effective lifetime (triangles), and the extrinsic recombination time (rectangles) *vs* excess concentration. Experimental data (symbols) and the calculated ones (line).

Sachenko A.V., Kostylyov V.P., Korkishko R.M. et al. Key parameters of textured silicon solar cells of 26.6% ...

Table. Parameters obtained by fitting the experimental results from [4].

S_{0s}	r	τ_{SRH}	τ_R	x_m	σ	b_r	R_{sh}	R_s
0.031 cm/s	2	15.2 ms	14 μs	0.25 μm	45 nm	0.1	$1.48 \cdot 10^5$ Ω·cm²	0.19 Ω·cm²

Let us calculate the dependences $\tau_{eff}\left(\Delta n_{OC}\right)$ more accurately, taking into account the effect of bands narrowing, and also correctly find the value of the shunt resistance R_{sh}.

To do this, we use the experimental illuminance – open-circuit voltage dependence, shown in Fig. 3, taken from Fig. 4b of the work [4]. In this work, the illumination level is normalized to the value of the sun illumination under the conditions of AM1.5. The theoretical dependence $Suns\left(V_{OC}\right)$ was constructed using the joint solution of equations (21), (22), and the value of the light intensity was obtained by normalizing the photogenerated current density J_L to 0.0425 A/cm². The theoretical dependence coincided with the experimental one, if using the varied parameters shown in Table, in particular, at $R_{sh} = 1.48 \cdot 10^5$ Ω·cm².

Shown in Fig. 4 is the experimental dependence $\tau_{eff}\left(\Delta n_{OC}\right)$ (see blue curve, image in Fig. 4a of [4]). To obtain a theoretical dependence $\tau_{eff}\left(\Delta n_{OC}\right)$, we used the expression

$$\tau_{eff}\left(\Delta n_{OC}\right) = \frac{q\,d\,\Delta n_{OC}\left(V_{OC}\right)}{J_L\left(V_{OC}\right) + \dfrac{V_{OC}}{R_{sh}}}, \qquad (26)$$

and the dependence $n_{OC}\left(V_{OC}\right)$ was calculated from the joint solution of the equations (21) and (22). Using the expression (26), we obtained the calculated dependence $\tau_{eff}\left(\Delta n_{OC}\right)$ shown in Fig. 4. As can be seen from Fig. 4, in the region of $\Delta n_{OC} < 10^{15}\,cm^{-3}$, the calculated dependence obtained by us is consistent with the dependence given in [4]. At the same time, at $\Delta n_{OC} < 10^{15}\,cm^{-3}$, the dependence calculated by us is slightly higher than the dependence given in [4]. As noted above, the reason for this is related to the fact that the effect of narrowing the zones was not taken into account in [4].

The relation between the effective lifetime and the excitation level, obtained from Fig. 4b of [4], which take into account all possible recombination mechanisms (triangles), and the extrinsic lifetime $\tau_{extr}\left(\Delta n\right)$, which does not include the contributions of the band-to-band Auger recombination and radiative recombination (rectangles), are shown in Fig. 3. Note that, when

calculating the radiative lifetime to obtain $\tau_{extr} = \left(\tau_{eff}^{-1} - \tau_{rad}^{-1} - \tau_{Auger}^{-1}\right)^{-1}$, we took into account photon re-absorption, whereas in [4], photon re-absorption has been neglected. As can be seen from this figure, as well as from Fig. 4a of [4], at excitation levels Δn is greater than $10^{16}\,cm^{-3}$, both curves decrease with almost the same slope. It is easy to see that $\tau_{eff}(\Delta n)$ and $\tau_{extr}(\Delta n) \sim \Delta n^{-\beta}$, where β is close to 2. In the case of $\tau_{eff}(\Delta n)$ such a decrease is due to band-to-band Auger recombination. As for $\tau_{extr}(\Delta n)$, it can only be explained by surface recombination. Therefore, in this case, the exponent r in (17) is close to 2.

To explain this dependence, it should be borne in mind that the model of one recombination center close to the middle of the bandgap, which is responsible for surface recombination, is approximate. In particular, since studies performed for the Si-SiO₂ system have shown, in addition to discrete levels, there are two systems of continuously distributed donor-like and acceptor-like surface centers [19]. Their concentration $N_s(E)$ increases exponentially near the edges of the bandgap, and there in some instances the contribution of these surface centers to the net recombination rate may exceed the contribution of the deep level [20, 21]. If $\Delta n > N_d$, the electron quasi-Fermi level begins to shift in the direction of increasing $N_s(E)$, and this can lead to an additional increase in $S(\Delta n)$, as compared to the typical case when $r = 1$. A similar scenario can be realized when crystalline silicon boundaries on other dielectrics.

In Fig. 5, experimental and theoretical dependences for light I–V characteristics are shown. Eqs (17) and (20) were used in the theoretical modeling of light I–V characteristics. As can be seen from the figure, the agreement between theory and experiment is good for the varied parameters given in the table, in particular, when using a value for the series resistance equal to 0.19 Ω·cm².
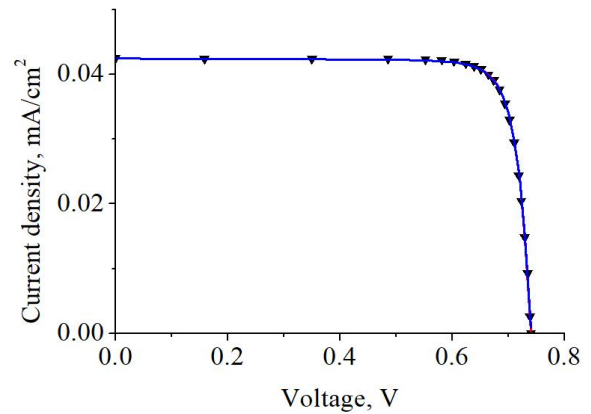
Fig. 5. The experimental data from [4] (triangles) and the theoretical I–V curve.

Sachenko A.V., Kostylyov V.P., Korkishko R.M. et al. Key parameters of textured silicon solar cells of 26.6% ...

180
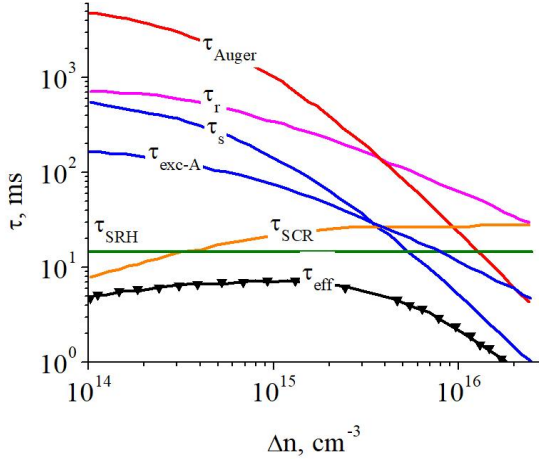
Fig. 6. The effective lifetime together with the individual contributions, as indicated near each curve, *vs* the excess concentration. The fitting parameters used to generate the theoretical curves are as follows: $\tau_{SRH} = 15.2$ μs, $S_{0s} = 0.031$ cm/s, $r = 2$, $\tau_{SCR} = 14$ μs, $\sigma = 45$ nm, $b_r = 0.1$, $R_{sh} = 1.48 \cdot 10^5$ Ω·cm^2, $R_s = 0.19$ Ω·cm^2.
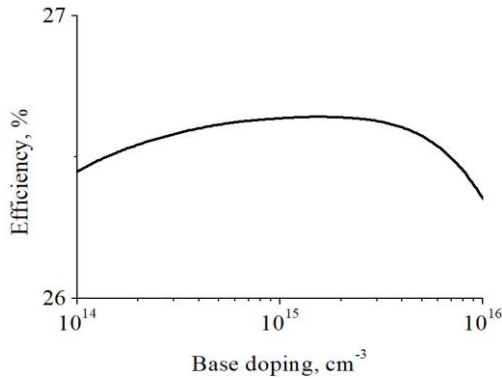
Fig. 7. The theoretical photoconversion efficiency *vs* base doping level at the base thickness $d = 200$ μm.

Using the parameters from Table and solving jointly (21), (22), we obtained for V_{OC} the calculated value of 740.3 mV, which coincides with the value given in [4]. Substitution of these parameters into the expressions for η and FF, we obtained the calculated values of 26.63% and 84.65%, respectively, which also completely coincide with the experimental data.

As always, the question arises as to how unambiguous the fitting parameters are. At a first glance, the fact that the Shockley–Reed–Hall recombination, surface recombination, and the SCR recombination rates are additive should lead to ambiguity. But each contribution depends on the excess concentration Δn differently. This avoids ambiguity. This point is illustrated in Fig. 6, which in addition to the dependence $\tau_{eff}(\Delta n)$ shows the contribution of surface recombination (τ_s), SCR recombination (τ_{SCR}), the SRH recombination (τ_{SRH}), the exciton non-radiative recombination (τ_{exc-A}), Auger band-to-band recombination (τ_{Auger}) and radiative recombination (τ_r). As can be seen from Fig. 6, at small values of Δn the greatest contribution to τ_{eff} comes from the SCR and SRH channels, and at large Δn – from the Auger and surface recombination. Interestingly, the contributions of exciton non-radiative recombination and radiative recombination depend on the value of Δn, but the contribution of the former is dominating.

Fig. 7 shows the calculated photoconversion efficiency *vs* the base doping level. As can be seen from the figure, the maximal efficiency of 26.64% is achieved at $N_d = 1.5 \cdot 10^{15}$ cm^{-3}. It differs by only 0.04% abs. from the value reported in [4].

Note that, using the results obtained in Section 2, we did not reach good agreement with the experimental short-circuit current density of 0.0425 A/cm^2, but also we can calculate the dependence of J_{SC} on the base thickness, which allows one to optimize the cell performance with respect to this parameter.

Fig. 8 shows the predicted curve η(d) obtained from the so obtained J_{SC} relation. The figure shows that the maximum efficiency of photoconversion is achieved at the base thickness close to 80 μm and reaches 26.86%, differing from the value obtained in [4] by 0.26%.

At the end of the paper, we will briefly dwell on the analysis of the case when the SRH recombination in silicon is determined by the gold impurities. Using the parameters of the two levels of gold in silicon, given in Graff's monograph [22]: $\sigma_{n1} = 1.4 \cdot 10^{-16}$, $\sigma_{p1} = 7.6 \cdot 10^{-15}$, $\sigma_{n2} = 2.7 \cdot 10^{-15}$, $\sigma_{p2} = 2.5 \cdot 10^{-15}$ cm^2, $E_{t1} = -0.55$ (the energy is measured from the bottom of the conduction band), $E_{t2} = 0.35$ eV (the energy is measured from the top of the valence band) , and the values of average thermal velocities for electrons and holes in silicon given in [23, 24], the following expression for $\tau_{SRH}(N_{Au})$ can be obtained at $T = 298.15$ K:

$$\tau_{SRH}(N_t, \Delta n) = \left[\frac{2.86 \cdot 1.27 \cdot 10^{-16} \left(6.5 \cdot 10^{14} + \Delta n\right) N_t}{2.86 \cdot 10^{-9} \left(6.5 \cdot 10^{14} + \Delta n + 1.54 \cdot 10^{10}\right) + 1.27 \cdot 10^{-7} \left(\Delta n + 6.07 \cdot 10^9\right)} + \right.$$

$$\left. + \frac{5.51 \cdot 4.19 \cdot 10^{-16} \left(6.5 \cdot 10^{14} + \Delta n\right) N_t}{5.51 \cdot 10^{-8} \left(6.5 \cdot 10^{14} + \Delta n + 2.65 \cdot 10^6\right) + 4.19 \cdot 10^{-8} \left(\Delta n + 3.53 \cdot 10^{13}\right)} \right]^{-1}. \qquad (27)$$

Sachenko A.V., Kostylyov V.P., Korkishko R.M. et al. Key parameters of textured silicon solar cells of 26.6% ...

181
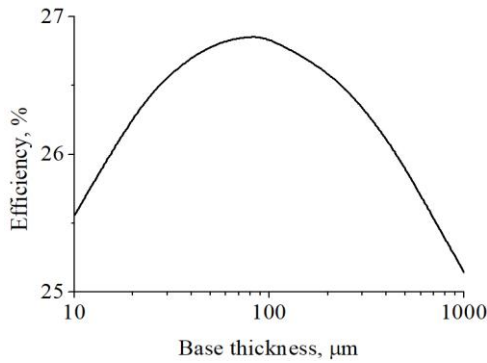
Fig. 8. The theoretical photoconversion efficiency *vs* base thickness at the base doping level $N_d = 6.5 \cdot 10^{14}$ cm^{-3}.

If we set the value of N_{Au} to $3.14 \cdot 10^9$ cm^{-3}, and S_{0s} to 0.0024 cm/s, then the calculated curve $\tau_{eff}(\Delta n)$ agrees well with the experimental one in the whole range of excess concentrations. In this case, we obtain a theoretical value of V_{OC} equal to 740.3 mV, and setting R_s to 0.23 Ω·cm^2, we obtain the efficiency of 26.63%. It can be noted that the concentration of gold in silicon of the order of $10^9 - 10^{10}$ cm^{-3} is quite realistic [22].

Thus, for SCs from [4], it is not possible to discriminate the mechanism that provides a decrease of $\tau_{eff}(\Delta n)$ at low Δn. Calculations have shown that this decline can be provided both by the SCR recombination and recombination in the bulk, for example, with participation of gold.

To discriminate this mechanism, experimenters can be advised to obtain dependences $\tau_{eff}(\Delta n)$ in the material that used to create SC. In this case, the boundary conditions on both surfaces of the sample will be the same, and the inversion bending of the zones on them will be absent. If the decreasing region of $\tau_{eff}(\Delta n)$ in the region of small Δn persists, this should be associated with the Shockley–Read–Hall recombination with participation of the gold level. If the descending region is absent, the decrease in $\tau_{eff}(\Delta n)$ in the operating device should be associated with recombination in SCR.

6. Conclusions

In this paper, a new approach to modeling the main parameters of high efficiency textured silicon solar cells is proposed. Unlike conventional optimization formalisms, which account for existing recombination mechanisms, the offered approach additionally includes such important factors as the non-radiative Auger recombination of excitons *via* deep impurity levels as well as electron-hole pairs recombination in the space charge region.

The proposed theoretical formalism allows us to well describe the experimental results for the heterojunction silicon solar cells with the record photoconversion efficiency of 26.6%. The expression for the SCR recombination velocity obtained here is valid both at small values of $\Delta n < N_d$ and at $\Delta n > N_d$. It has been shown that the contribution of the non-radiative

exciton Auger recombination *via* deep impurities exceeds the contribution of radiative recombination in the analyzed SCs. It has been ascertained that the experimentally observed decrease of the effective lifetime $\tau_{eff}(\Delta n)$ at small excess concentrations may be caused by either recombination in the space charge region or SHR recombination *via* gold impurities. The conditions under which one can discriminate between these two recombination mechanisms have been formulated. Finally, the simulation results are quantitatively consistent with the experimental data across the whole range of parameters. The discussion has taken into account the influence of shunt resistance on the dependence of short-circuit current – open-circuit voltage. The results obtained in this work can be used to optimize the characteristics of textured silicon SCs with respect to base doping level and thickness.

References

1. Hangleiter A. Nonradiative recombination *via* deep impurity levels in silicon: Experiment. *Phys. Rev. B.* 1987. **35**, No 17. P. 9149–9160. https://doi.org/10.1103/PhysRevB.35.9149.
2. Hangleiter A. Nonradiative recombination *via* deep impurity levels in semiconductors: The excitonic Auger mechanism. *Phys. Rev. B.* 1988. **37**, No 5. P. 2594–2604. https://doi.org/10.1103/physrevb.37.2594.
3. Abakumov V.N., Perel V.l., Yassievich I.N. *Nonradiative Recombination in Semiconductors.* Elsevier, 1991.
4. Yoshikawa K., Yoshida W., Irie T. *et al.* Exceeding conversion efficiency of 26% by heterojunction interdigitated back contact solar cell with thin film Si technology. *Solar Energy Materials and Solar Cells.* 2017. **173**. P. 37–42. https://doi.org/10.1016/j.solmat.2017.06.024.
5. Yoshikawa K., Kawasaki H., Yoshida W. *et al.* Silicon heterojunction solar cell with inter-digitated back contacts for a photoconversion effciency over 26%. *Nature Energy.* 2017. **2**, No 5. P. 17032, 8 p. https://doi.org/10.1038/nenergy.2017.32.
6. Green M.A., Dunlop E.D., Hohl-Ebinger J. *et al.* Solar cell efficiency tables (Version 55). *Progress in Photovoltaics.* 2020. **28**, No 1. P. 3-15. https://doi.org/10.1002/pip.3228.
7. McIntosh K.R., Baker-Finch S.C. A parameterization of light trapping in wafer-based solar cells. *IEEE J. Photovolt.* 2015. **5**, No 6. P. 1563–1570. https://doi.org/10.1109/JPHOTOV.2015.2465175.
8. Fell A., McIntosh K.R., Fong K.C. Simplified device simulation of silicon solar cells using a lumped parameter optical model. *IEEE J. Photovoltaics.* 2016. **6**, No 3. P. 611–616. https://doi.org/10.1109/JPHOTOV.2016.2528407.
9. Sachenko A.V., Kostylyov V.P., Bobyl A.V. *et al.* The effect of base thickness on photoconversion efficiency in textured silicon-based solar cells. *Techn. Phys. Lett.* 2018. **44**. P. 873–876. https://doi.org/10.1134/S1063785018100139.

Sachenko A.V., Kostylyov V.P., Korkishko R.M. et al. Key parameters of textured silicon solar cells of 26.6% ...

182

10. Sachenko A.V., Kostylyov V.P., Vlasyuk V.M., Sokolovskyi I.O., and Evstigneev M. Optimization of textured silicon solar cells. *47th IEEE Photovoltaic Specialists Conference*, Canada, Calgary, 15-21 June 2020.

11. Sachenko A.V., Kostylyov V.P., Vlasyuk V.M., Sokolovskyi I.O., and Evstigneev M. The influence of the exciton nonradiative recombination in silicon on the photoconversion efficiency. *Proc. 32 European Photovoltaic Solar Energy Conference and Exhibition*, Germany, Munich, 20-24 June 2016, pp. 141–147.

12. Richter A., Glunz S. W., Werner F., Schmidt J., and Cuevas A. Improved quantitative description of Auger recombination in crystalline silicon. *Phys. Rev. B.* 2012. **86**, No 16. P. 165202, 14 p. https://doi.org/10.1103/PhysRevB.86.165202.

13. Richter A., Hermle M., and Glunz S.W. Reassessment of the limiting efficiency for crystalline silicon solar cells. *IEEE J. Photovolt.* 2013. **3**, No 4. P. 1184–1191. https://doi.org/10.1109/JPHOTOV.2013.2270351.

14. Richter A., Benick J., Feldmann F., Fell A., Hermle M., Glunz S.W. *n*-Type Si solar cells with passivating electron contact: identifying sources for efficiency limitations by wafer thickness and resistivity variation. *Solar Energy Materials and Solar Cells.* 2017. **173**. P. 96–105. https://doi.org/10.1016/j.solmat.2017.05.042.

15. Sachenko A.V., Kostylyov V.P., Vlasiuk V.M. *et al.* Features in the formation of recombination current in the space charge region of silicon solar cells. *Ukr. J. Phys.* 2016. **61**, No 10. P. 917–922. https://doi.org/10.15407/ujpe61.10.0917.

16. Sachenko A.V., Kostylyov V. P., Sokolovskyi I.O. *et al.* Specific features of current flow in α-Si: H/Si heterojunction solar cells. *Techn. Phys. Lett.* 2017. **43**. P. 152–155. https://doi.org/10.1134/S1063785017020109.

17. Sproul A.B. and Green M.A. Intrinsic carrier concentration and minority-carrier mobility of silicon from 77 to 300 K. *J. Appl. Phys.* 1993. **73**. P. 1213. https://doi.org/10.1063/1.353288.

18. Schenk A. Finite-temperature full random-phase approximation mode of band gap narrowing for silicon device simulation. *J. Appl. Phys.* 1998. **84**. P. 3684–3695. https://doi.org/10.1063/1.368545.

19. Lytovchenko V.H., Gorban A.P. *Fundamentals of Physics of Microelectronic Systems Metal–Dielectric–Semiconductor.* Kiev, Naukova dumka, 1978 (in Russian).

20. Kostylyov V.P., Sachenko A.V., Sokolovskyi I.O. Influence of surface centers on the effective surface recombination rate and the parameters of silicon solar cells. *Ukr. J. Phys.* 2013. **58**, No 4. P. 362–369. https://doi.org/10.15407/ujpe58.04.0362.

21. McIntosh K.R., Black L.E. On effective surface recombination parameters. *J. Appl. Phys.* 2014. **116**. P. 014503. https://doi.org/10.1063/1.4886595.

22. Graff K. Metal Impurities in Silicon-Device Fabrication. *Springer Series in Materials Science.* 2000. **24**. Berlin, Springer-Verlag. https://doi.org/10.1007/978-3-642-57121-3.

23. Green M.A. Intrinsic concentration, effective densities of states, and effective mass in silicon. *J. Appl. Phys.* 1990. **67**, No 6. P. 2944–2955. https://doi.org/10.1063/1.345414.

24. Gorban A.P., Zuev V.A., Kostylyov V.P., Sachenko A.V., Serba A.A., Chernenko V.V. About temperature dependences of equilibrium and non-equilibrium characteristics in silicon. *Optoelectronics and Semiconductor Technique.* 2001. **36**. P. 161–165 (in Russian).

Authors and CV

Sachenko A.V. Professor, Doctor of Physics and Mathematics Sciences, Chief Researcher of the Laboratory of Physical and Technical Fundamentals of Semiconductor Photovoltaics at the V. Lashkaryov Institute of Semiconductor Physics. He is the author of more than 300 scientific publications. His main research interests include analysis, characterization, and modeling of silicon solar cells.

Kostylyov V.P. Professor, Doctor of Physics and Mathematics Sciences, Head of the Laboratory of Physical and Technical Fundamentals of Semiconductor Photovoltaics at the V. Lashkaryov Institute of Semiconductor Physics. He is the author of more than 250 scientific publications. The area of his scientific interests includes development of equipment for silicon solar cells testing, research, analysis of silicon solar cells.

Korkishko R.M. PhD, Researcher of the Laboratory of Physical and Technical Fundamentals of Semiconductor Photovoltaics at the V. Lashkaryov Institute of Semiconductor Physics. He is the author of more than 63 scientific publications. The area of his scientific interests includes research, analysis of silicon solar cells.

Vlasyuk V.M. PhD, Researcher of the Laboratory of Physical and Technical Fundamentals of Semiconductor Photovoltaics at the V. Lashkaryov Institute of Semiconductor Physics. He is the author of more than 47 scientific publications. The area of his scientific interests includes research, analysis of silicon solar cells.

Sachenko A.V., Kostylyov V.P., Korkishko R.M. et al. Key parameters of textured silicon solar cells of 26.6% ...

183

Sokolovskyi I.O. PhD, Senior Researcher of the Laboratory of Physical and Technical Fundamentals of Semiconductor Photovoltaics at the V. Lashkaryov Institute of Semiconductor Physics. He is the author of more than 70 scientific publications. His main research interests include modeling of silicon solar cells.

Chernenko V.V. PhD, Senior Researcher of the Laboratory of Physical and Technical Fundamentals of Semiconductor Photovoltaics at the V. Lashkaryov Institute of Semiconductor Physics. He is the author of more than 100 scientific publications. His main research interests include research, analysis of silicon solar cells.

Dvernikov B.F. Researcher of the Laboratory of Physical and Technical Fundamentals of Semiconductor Photovoltaics at the V. Lashkaryov Institute of Semiconductor Physics. The area of his scientific interests includes manufacturing of equipment for silicon solar cells testing.

Evstigneev M.A. PhD, Assistant Professor of the faculty of Physics and Physical Oceanography at the Memorial University of Newfoundland. His research areas are non-equilibrium statistical physics, biophysics, surface science.

Ключові параметри текстурованих кремнієвих сонячних елементів з ефективністю 26,6%

А.В. Саченко, В.П. Костильов, Р.М. Коркішко, В.М. Власюк, І.О. Соколовський, Б.Ф. Дверніков, В.В. Черненко, М. Євстігнєєв

Анотація. Представлено новий підхід до моделювання параметрів високоефективних текстурованих кремнієвих сонячних елементів. На відміну від інших алгоритмів оптимізації, наш підхід додатково включає такі важливі чинники, як безвипромінювальна оже-рекомбінація екситонів крізь глибокі домішкові рівні, а також рекомбінація електронно-діркових пар в області просторового заряду. Також використовується простий феноменологічний вираз, який ми запропонували для зовнішньої квантової ефективності текстурованого кремнієвого сонячного елемента в довгохвильовій частині спектра поглинання. За допомогою цього підходу теоретично визначаються такі ключові параметри текстурованих кремнієвих сонячних елементів, як струм короткого замикання, напруга розімкнутого кола та ефективність фотоперетворення. Запропонований підхід дозволяє розрахувати залежність ефективності фотоперетворення від товщини, що добре узгоджується з експериментальними результатами, отриманими для гетеропереходних сонячних елементів з рекордною ефективністю фотоперетворення 26,6%. Запропонований підхід може бути використаний для оптимізації характеристик високоефективних текстурованих сонячних елементів на основі монокристалічного кремнію.

Ключові слова: кремнієвий сонячний елемент, текстура, напруга розімкненого кола, густина струму короткого замикання, ефективність фотоперетворення, коефіцієнт заповнення.

Sachenko A.V., Kostylyov V.P., Korkishko R.M. et al. Key parameters of textured silicon solar cells of 26.6% ...

184